

## Deciphering the relative contribution of vascular inflammation and blood rheology in metastatic spreading

Hilaria Mollica,<sup>1,2</sup> Alessandro Coclite,<sup>2</sup> Marco E. Miali,<sup>2,3</sup> Rui C. Pereira,<sup>2</sup> Laura Paleari,<sup>4,5</sup> Chiara Manneschi,<sup>2</sup> Andrea DeCensi,<sup>4,6</sup> and Paolo Decuzzi<sup>2,a)</sup>

<sup>1</sup>*DIBRIS, University of Genova, Via Opera Pia 13, Genoa 16145, Italy*

<sup>2</sup>*Laboratory of Nanotechnology for Precision Medicine, Fondazione Istituto Italiano di Tecnologia, Via Morego 30, Genoa 16163, Italy*

<sup>3</sup>*Dipartimento di Meccanica, Matematica e Management, DMMM, Politecnico di Bari, Via Re David, 200-70125 Bari, Italy*

<sup>4</sup>*Division of Medical Oncology, Galliera Hospital, Via Volta 6, Genoa 16128, Italy*

<sup>5</sup>*A.Li.Sa, Public Health Agency, Piazza della Vittoria 15, Genoa 16121, Italy*

<sup>6</sup>*Wolfson Institute of Preventive Medicine, Queen Mary University of London, Charterhouse Square, London EC1M 6BQ, United Kingdom*

(Received 19 January 2018; accepted 2 April 2018; published online 17 May 2018)

Vascular adhesion of circulating tumor cells (CTCs) is a key step in cancer spreading. If inflammation is recognized to favor the formation of vascular “metastatic niches,” little is known about the contribution of blood rheology to CTC deposition. Herein, a microfluidic chip, covered by a confluent monolayer of endothelial cells, is used for analyzing the adhesion and rolling of colorectal (HCT-15) and breast (MDA-MB-231) cancer cells under different biophysical conditions. These include the analysis of cell transport in a physiological solution and whole blood over a healthy and a TNF- $\alpha$  inflamed endothelium with a flow rate of 50 and 100 nl/min. Upon stimulation of the endothelial monolayer with TNF- $\alpha$  (25 ng/ml), CTC adhesion increases from 2 to 4 times whilst cell rolling velocity only slightly reduces. Notably, whole blood also enhances cancer cell deposition from 2 to 3 times, but only on the unstimulated vasculature. For all tested conditions, no statistically significant difference is observed between the two cancer cell types. Finally, a computational model for CTC transport demonstrates that a rigid cell approximation reasonably predicts rolling velocities while cell deformability is needed to model adhesion. These results would suggest that, within microvascular networks, blood rheology and inflammation contribute similarly to CTC deposition, thereby facilitating the formation of metastatic niches along the entire network, including the healthy endothelium. In microfluidic-based assays, neglecting blood rheology would significantly underestimate the metastatic potential of cancer cells.

Published by AIP Publishing. <https://doi.org/10.1063/1.5022879>

### I. INTRODUCTION

The formation of distant metastasis from a primary neoplastic mass is a very inefficient biological process (Talmadge and Fidler, 2010; Nguyen *et al.*, 2009; Wirtz *et al.*, 2011; and Joyce and Pollard, 2009). Spreading of cancer cells evolves following a precise cascade of events—the metastatic cascade—requiring cell migration away from the primary mass and intravasation into blood or lymphatic vessels, following the epithelial to mesenchymal transition; circulation within the blood stream, where cells have to survive hemodynamic stresses and immune cell recognition; extravasation, migration, and proliferation at the secondary sites. Radioactive assays documented that only 1% of circulating tumor cells (CTCs) can successfully overcome all these

---

<sup>a)</sup>Author to whom correspondence should be addressed: Paolo.Decuzzi@iit.it. Tel.: +39 010 71781 941. Fax: +39 010 71781 228

sequential steps and eventually establish distant metastases (Fidler, 1970). Despite the inefficiency and complexity of the process, the vast majority of cancer patients who relapse eventually succumb because of metastases, disseminated at different secondary sites, rather than for the uncontrolled growth of the original malignancy (Chaffer and Weinberg, 2011).

CTC arrest within different vascular districts is a key step in the metastatic cascade and is primarily mediated by two mechanisms: vascular occlusion, which generally occurs in the small capillary beds of the brain and lungs (Kienast *et al.*, 2010), and vascular adhesion, which is regulated by specific interactions between receptor molecules on the endothelium and ligand molecules on CTCs (Schluter *et al.*, 2006; Witz, 2008). A wide range of vascular molecules are involved in this specific adhesion process, including E- and P-selectins,  $\alpha_v\beta_3$  and  $\alpha_v\beta_5$  integrins, VCAM-1 and ICAM-1 adhesion molecules (Burdick *et al.*, 2003; Barthel *et al.*, 2007; and Myung *et al.*, 2011). These receptors can bind several different ligands expressed on the CTC membrane, making target therapies against metastasis practically impossible. This picture is further complicated by the fact that platelets, leukocytes, and CTCs tend to form in the circulation stable aggregates that favor blood longevity and vascular deposition of malignant cells (Gay and Felding-Habermann, 2011; Borsig *et al.*, 2002). In this context, pro-inflammatory cytokines (Solinas *et al.*, 2010; Kim *et al.*, 2009), such as TNF- $\alpha$ , IL-1 $\beta$ , and IL-6, tumor-derived exosomes (Hoshino *et al.*, 2015; Hood *et al.*, 2011), and hematopoietic cells (Kaplan *et al.* 2005; Shiozawa *et al.*, 2011) have been shown to modulate the expression of adhesion molecules in specific vascular districts, thus priming the formation of so called “pre-metastatic niches” where CTCs more efficiently, and in a larger number, accumulate.

Cell-cell adhesion is strongly modulated by external forces and, as such, static assays may not always reproduce the complex interactions developing under flow within the vasculature. Intravital microscopy has been extensively employed to document cell migration within vascular and extravascular compartments (Kienast *et al.*, 2010; Provenzano *et al.*, 2009); however, these *in vivo* analyses lack a precise control on the governing parameters. On the other hand, microfluidic chips allow to precisely control blood vessel sizes, flow rates, and the expression of vascular adhesion molecules and are amenable for high through-put systematic characterizations. A variety of microfluidic chips are being developed for studying the different steps in the metastatic cascade. For instance, the group of Kamm designed flow devices for assessing transvascular migration of cancer cells in different extravascular matrices (Bersini *et al.*, 2014; Jeon *et al.*, 2015; Niu *et al.*, 2014; and Zervantonakis *et al.* 2012). The vascular adhesion and transmigration of individual and clustered CTCs were studied under chemokine stimulation (exposure to CXCL12 and SDF-1 $\alpha$ ) by various groups (Song *et al.*, 2009; Zhang *et al.*, 2012; and Roberts *et al.*, 2016). Studies of cancer cell migration within the lymphatic system were presented by Swartz and collaborators (Pisano *et al.*, 2015). The group of Jiang focused on investigating the role of endothelial cell mechanical (cyclic shear stresses) and biochemical (exposure to TNF- $\alpha$ ) stimulation on CTC vascular adhesion (Huang *et al.*, 2015). Huang and collaborators developed cellulose-based tubular artificial blood vessels for reproducing the intravasation, vascular adhesion and extravasation of cancer cells (Wang *et al.*, 2015).

Although red blood cells (RBCs) are known to affect the dynamics of leukocytes and CTCs, at authors' knowledge, no studies have addressed the relative roles of vascular inflammation and RBC dynamics on the vascular deposition of malignant cells. In this work, a microfluidic chip is used to study the rolling and firm adhesion of breast (MDA-MB-231) and colorectal cancer (HCT-15) cells on a confluent layer of human vascular endothelial cells (HUVECs). The hematocrit of the working solution ranges from 0% to 40% and TNF- $\alpha$  is used for stimulating HUVECs. The rolling velocity and number of firmly adhering tumor cells are measured under different conditions. A Lattice-Boltzmann computational model is also included to interpret and reproduce the vascular adhesion dynamics of cells.

## II. RESULTS AND DISCUSSIONS

A continuously growing body of evidence documents that vascular inflammation supports the firm adhesion of circulating tumor cells (CTCs) and facilitate the distant colonization of

otherwise healthy tissues with the consequent formation of tumor metastases (Solinas *et al.*, 2010; Kim *et al.*, 2009; Hoshino *et al.*, 2015; and Hood *et al.*, 2011). In this context, human vascular endothelial cells (HUVECs) were stimulated with the pro-inflammatory cytokine TNF- $\alpha$ , and the adhesion propensity of cancer cells (HCT-15 and MDA-MB-231) was assessed under static and dynamic conditions. The two cell lines are among the most metastatic and aggressively growing colon and breast cancer cells, respectively (Flatmark *et al.*, 2004; Holliday and Speirs, 2011).

### A. Cancer cell adhesion on inflamed endothelial cells under dynamic conditions

HUVECs were seeded in multiwell plates and, after reaching confluency, were stimulated with TNF- $\alpha$  (10 ng/ml, 25 ng/ml, 50 ng/ml) for 6 h. Cancer cells were added to the multiwell plates and left interacting with the endothelial cells up to 4 h, under static conditions. In agreement with a large body of literature, these static experiments continue to confirm that endothelial stimulation with a pro-inflammatory cytokine (TNF- $\alpha$ ) favors CTC vascular adhesion in a dose dependent manner (supplementary Figs. 1 and 2). Moving from static to dynamic experimental conditions, a PDMS single-channel microfluidic chip was used for monitoring the interaction of cancer and endothelial cells under flow [Fig. 1(a)]. The microfluidic channel was 2.7 cm long and had a 210  $\mu\text{m}$  wide  $\times$  42  $\mu\text{m}$  high rectangular cross section. The working fluid was introduced in the PDMS chip continuously for about 15 min at two different flow rates, namely, 50 and 100 nl/min. These flow rates reproduce wall shear rates (13.49 and 26.99  $\text{s}^{-1}$ ) and mean blood velocities (94.48 and 188.9  $\mu\text{m/s}$ ) typically found in the microcirculation (Popel and Johnson, 2005). The PDMS channel was covered by a confluent layer of endothelial cells mimicking the blood vessel walls; whereas the cancer cells were dispersed within the working fluid consisting of either cell culture media or whole blood. Again, two different malignant cell lines were considered, namely, colon (HCT-15) and breast cancer (MDA-MB-231) cells. In

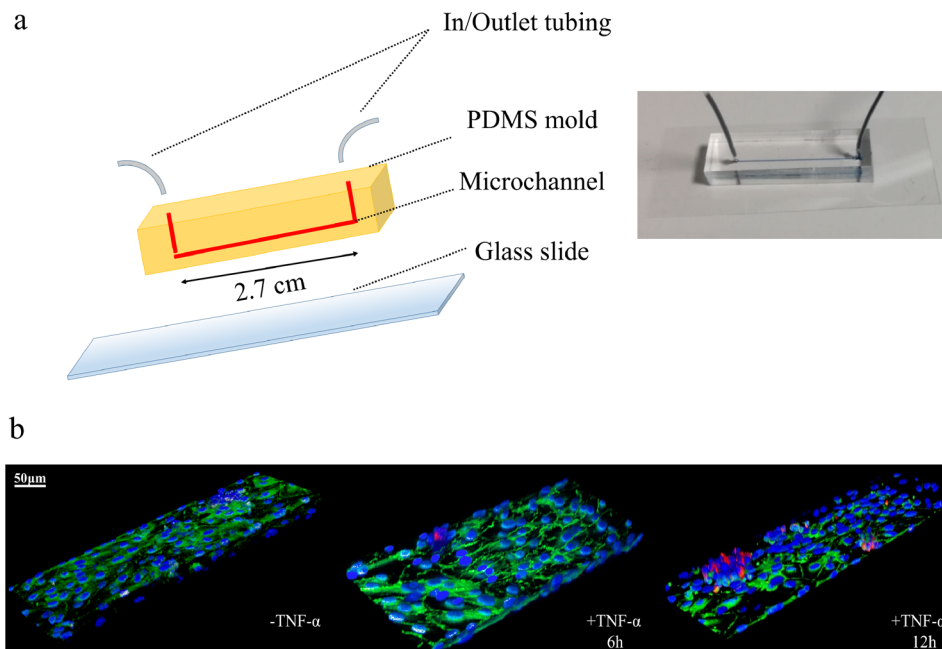


FIG. 1. Single-channel microfluidic chip. (a) On the left, schematic representation of a single channel microfluidic chip with length  $l = 2.7$  cm, width  $w = 210$   $\mu\text{m}$ , and height  $h = 42$   $\mu\text{m}$ . On the right, a single channel microfluidic chip, with connecting inlet and outlet tubing, filled with a blue ink and placed on the stage of a fluorescent inverted microscope. (b) Representative confocal fluorescence microscopy images of HCT-15 cells (membrane labeled in red with CM-DIL) flowing in the chip and interacting with a confluent layer of HUVECs (nuclei stained in blue with DAPI). VE-cadherin adhesion molecules, arising at boundaries of the endothelial cells, are stained in green [Images are provided for unstimulated (-TNF- $\alpha$ ) and TNF- $\alpha$  stimulated HUVECs for 6 (+TNF- $\alpha$  6h) and 12 h (+TNF- $\alpha$  12h). TNF- $\alpha$  concentration: 25 ng/ml. Scale bar: 50  $\mu\text{m}$ ].

order to reproduce an inflamed endothelium, the HUVEC monolayer was stimulated with the pro-inflammatory cytokine TNF- $\alpha$ . Representative confocal fluorescent images of the experimental setup with cells are shown in Fig. 1(b). Red fluorescent cancer cells (CM-DIL staining of the membrane) are spotted firmly adhering over blue fluorescent HUVECs (DAPI staining of the nucleus). The same images show in green VE-cadherin molecules decorating the boundary between two adjacent endothelial cells and demonstrating the high level of confluency of the endothelial monolayer deposited on the microfluidic channel surface.

Via fluorescent microscopy, the number of adhering cells was quantified, within five different regions of interest (ROIs) along the channel, and normalized by the total number of injected cells ( $n_{inj} = 10^6$ ) and the ROI area. This was performed for 12 different working conditions depending on the types of cancer (colon and breast), flow rates (50 and 100 nl/min), and levels of HUVEC inflammation (un-stimulated: -TNF- $\alpha$ ; 6 h stimulation: +TNF- $\alpha$  6h; and 12h stimulation: +TNF- $\alpha$  12 h). The results are provided in Figs. 2(b) and 2(d), respectively, for a flow rate  $Q = 50$  and 100 nl/min, and for breast cancer (blue bars) and colon cancer (red bars) cells. On the left hand side, Figs. 2(a) and 2(c), representative fluorescent microscopy images are shown for unstimulated, 6 h stimulated, and 12 h stimulated HUVECs. These images are snapshots taken from full movies available in [supplementary material](#). Notably, for all 12 different working conditions, no statistically significant difference was depicted when comparing breast and colon cancer cells. Conversely, significant differences arose when considering different flow rates and levels of TNF- $\alpha$  stimulation. At  $Q = 50$  nl/min, the normalized number of

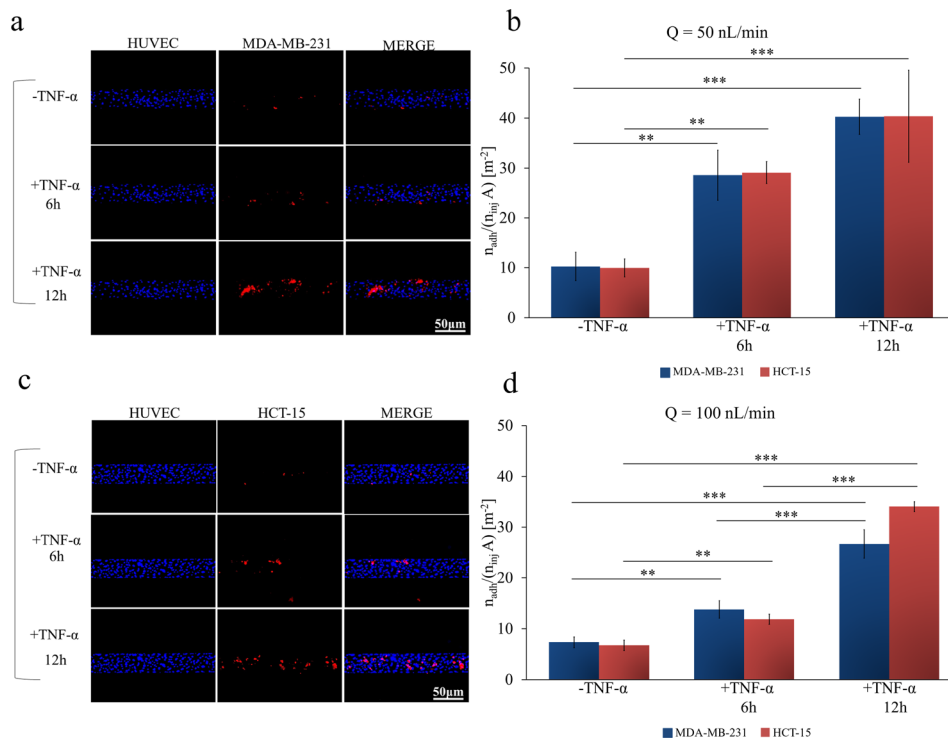


FIG. 2. Cancer cell adhesion on inflamed endothelial cells under dynamic conditions. (a) Representative fluorescence microscopy images of breast cancer cells MDA-MB-231 (cell membrane labeled in red with CM-DIL) flowing and interacting, in a single-channel microfluidic chip, with a confluent monolayer of HUVECs (cell nuclei stained in blue with DAPI). (b) Normalized number of adhering cancer cells on a HUVEC monolayer at a flow rate of 50 nl/min, with and without stimulation with TNF- $\alpha$  (25 ng/ml), for 6 and 12h. (c) Representative fluorescence microscopy images of colon cancer cells HCT-15 (cell membrane labeled in red with CM-DIL) flowing and interacting in a single-channel microfluidic chip, with a confluent monolayer of HUVECs (cell nuclei stained in blue with DAPI). (d) Normalized number of adhering cancer cells on a HUVEC monolayer at a flow rate of 100 nl/min, with and without stimulation with TNF- $\alpha$  (25 ng/ml), for 6 and 12h [Data are plotted as mean  $\pm$  SD.  $n = 3$ . Statistical analysis ANOVA: \*\*\* symbol denotes statistically significant difference  $p < 0.0001$ ; \*\* symbol denotes statistically significant difference  $p < 0.001$ . ( $n_{inj} = 10^6$  cells and  $A = 1.22 \times 10^{-6} \text{ m}^2$ ). HUVECs are not stimulated with TNF- $\alpha$  (-TNF- $\alpha$ ) or stimulated with 25 ng/ml TNF- $\alpha$  for 6h (+TNF- $\alpha$  6h) or 12h (+TNF- $\alpha$  12h)].

adhering HCT-15 and MDA-MB-231 cells was  $9.952 \pm 1.803$  and  $10.24 \pm 2.841$   $\#/m^2$  in control experiments,  $29.09 \pm 2.219$  and  $28.54 \pm 5.038$   $\#/m^2$  after 6 h of TNF- $\alpha$  stimulation; and  $40.37 \pm 9.205$  and  $40.26 \pm 3.521$   $\#/m^2$  after 12 h of TNF- $\alpha$  stimulation, respectively. At  $Q = 100$  nl/min, the normalized number of adhering HCT-15 and MDA-MB-231 cells was  $6.698 \pm 1.452$  and  $7.30 \pm 1.088$   $\#/m^2$  in control experiments,  $11.87 \pm 0.899$  and  $13.78 \pm 1.716$   $\#/m^2$  after 6 h of TNF- $\alpha$  stimulation; and  $34.05 \pm 1.427$  and  $26.69 \pm 2.780$   $\#/m^2$  after 12 h of TNF- $\alpha$  stimulation, respectively.

As compared to the healthy vasculature, cancer cells adhered 2 and 3-times more avidly to a 6 h- and 12 h-inflamed endothelium. Maximum cell adhesion is observed under static conditions [ $Q = 0$ , supplementary Fig. 1(c)], followed by  $Q = 50$  and 100 nl/min. Thus, as expected, the number of adhering cells reduces as the flow rate increases. Indeed, this is related to the corresponding increase in the hydrodynamic dislodging forces that would decrease the likelihood of firm CTC adhesion on HUVECs.

## B. Cancer cell rolling on inflamed endothelial cells under dynamic conditions

A subset of circulating tumor cells was observed to interact with the endothelial monolayer without firmly adhering but rather rolling steadily. The cancer cells exposed to dynamic conditions are transported within the microfluidic chip at two different flow rates (50 and 100 nl/min). The solution is injected into the microfluidic chip using a syringe pump for 15 min. Thus, the rolling velocity  $u_{roll}$  of tumor cells was quantified by monitoring the displacement of the cell centroid over time. Movies for rolling cells are provided in the [supplementary material](#) under different flow rates, HUVEC inflammation levels, and cell types. By imaging post-processing,  $u_{roll}$  of the metastatic colon (HCT-15) and breast (MDA-MB-231) cancer cells was quantified at 50 and 100 nl/min, and under different HUVEC conditions, namely, unstimulated HUVECs (-TNF- $\alpha$ ), 6h-stimulated HUVECs (+TNF- $\alpha$  6 h), and 12 h-stimulated HUVECs (+TNF- $\alpha$  12h). Data are charted in Figs. 3(a) and 3(b) for 50 and 100 nl/min, respectively. At 50 nl/min, the rolling velocity of HCT-15 cells was of  $113.9 \pm 4.132$ ,  $103.4 \pm 2.880$ , and  $98.00 \pm 4.552$   $\mu m/s$  for unstimulated HUVECs (-TNF- $\alpha$ ), 6 h-stimulated HUVECs (+TNF- $\alpha$  6 h), and 12 h-stimulated HUVECs (+TNF- $\alpha$  12 h), respectively. Under the same conditions, for the MDA-MB-231, the rolling velocities were  $118.6 \pm 1.349$   $\mu m/s$ ,  $105.68 \pm 3.340$   $\mu m/s$ , and  $102.1 \pm 5.288$   $\mu m/s$  [Fig. 3(a)]. Even in the case of rolling velocities, no statistically significant difference was observed between the two cell lines. A 10% and 20% statistically significant decrease in rolling velocities between the control groups and the 6 and 12 h TNF- $\alpha$  stimulated groups was observed. Under TNF- $\alpha$  stimulation, endothelial cells express a larger number of adhesion molecules, which would reduce the rolling velocity and favor the firm deposition of CTCs. Note that this is in agreement with what was documented by Navarro and collaborators (Ríos-Navarro *et al.*, 2015) in the case of polymorphonuclear (PMNCs) and peripheral blood mononuclear (PBMCs) cells.

As expected, the rolling velocity slightly but steadily decreased as the level of TNF- $\alpha$  stimulation increased. At 100 nl/min, the rolling velocities for the HCT-15 cells were  $163.6 \pm 20.10$   $\mu m/s$  (-TNF- $\alpha$ ),  $157.4 \pm 4.531$   $\mu m/s$  (TNF- $\alpha$  6 h), and  $158.06 \pm 1.187$   $\mu m/s$  (TNF- $\alpha$  12 h). For the MDA-MB-231, the same physical quantity took the values  $170.9 \pm 11.03$   $\mu m/s$  (-TNF- $\alpha$ );  $151.8 \pm 8.182$   $\mu m/s$  (6 h TNF- $\alpha$ ); and  $144.9 \pm 1.500$   $\mu m/s$  (12 h TNF- $\alpha$ ).

Finally, the ratio between the number of rolling and adhering cells was plotted for two different flow conditions [Figs. 3(c) and 3(d)]. For unstimulated HUVECs, most of the circulating tumor cells were observed to steadily roll over the endothelium monolayer, whereas the ratio decreases as the TNF- $\alpha$  stimulation increases. At low flow rates ( $Q = 50$  nl/min), the ratio for the HCT-15 cells was  $0.845 \pm 0.084$  (-TNF- $\alpha$ );  $0.713 \pm 0.122$  (TNF- $\alpha$  6 h) and  $0.553 \pm 0.096$  (TNF- $\alpha$  12 h). Very similar are the ratios quantified for the MDA-MB-231, for which it resulted as follows:  $0.828 \pm 0.067$  (-TNF- $\alpha$ ),  $0.669 \pm 0.034$  (TNF- $\alpha$  6 h), and  $0.597 \pm 0.030$  (TNF- $\alpha$  12 h). At high flow rates ( $Q = 100$  nl/min), the ratio for the HCT-15 cells was  $0.875 \pm 0.020$  (-TNF- $\alpha$ ),  $0.728 \pm 0.038$  (TNF- $\alpha$  6 h), and  $0.591 \pm 0.017$  (TNF- $\alpha$  12 h). Similarly, for the MDA-MB-231, the ratio was  $0.850 \pm 0.061$  (-TNF- $\alpha$ ),  $0.715 \pm 0.015$  (TNF- $\alpha$  6 h), and

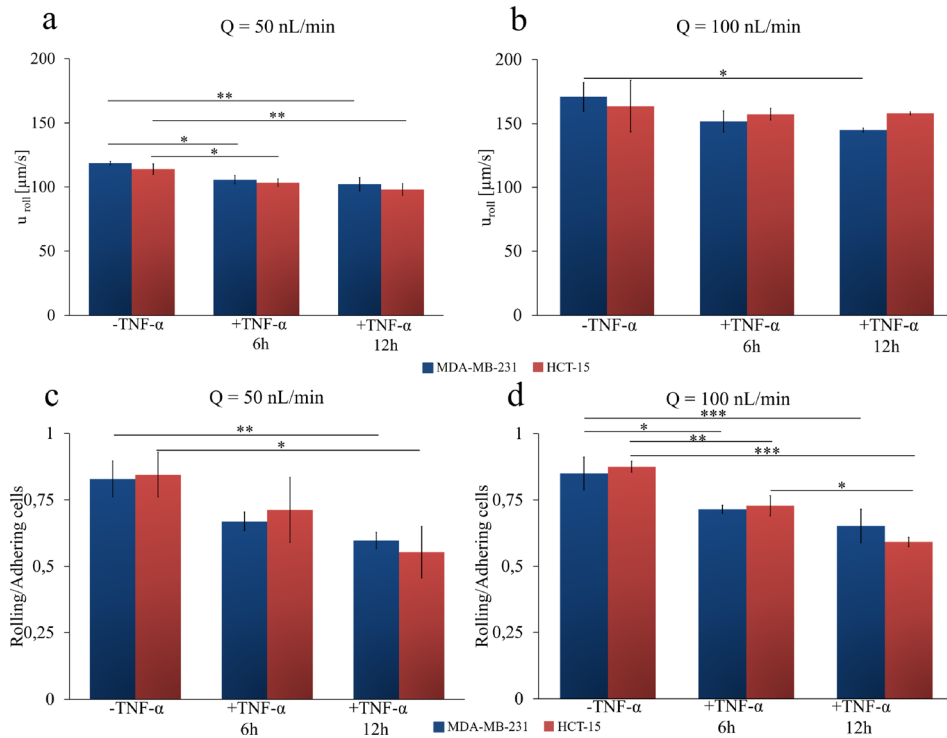


FIG. 3. Cancer cell rolling on inflamed endothelial cells under dynamic conditions. (a) and (b) Rolling velocity of colon cancer HCT-15 (red column) and breast cancer MDA-MB-231 (blue column) at 50 nl/min and 100 nl/min on a confluent layer of HUVECs. (c) and (d) Ratio between the number of rolling and adhering cancer cells (HCT-15—red column and breast cancer MDA-MB-231—blue column) on a confluent layer of HUVECs at 50 nl/min and 100 nl/min. HUVECs are not stimulated with TNF- $\alpha$  (-TNF- $\alpha$ ) or stimulated with 25 ng/ml of TNF- $\alpha$  for 6h (+TNF- $\alpha$  6h) or 12h (+TNF- $\alpha$  12h) (Data are plotted as mean  $\pm$  SD. n = 3. Statistical analysis ANOVA. \* symbol denotes statistically significant difference  $p < 0.01$ ; \*\* symbol denotes statistically significant difference  $p < 0.001$ ; \*\*\* symbol denotes statistically significant difference  $p < 0.0001$ ).

$0.651 \pm 0.063$  (TNF- $\alpha$  12 h). As reported before for other physical quantities, also in this case, no statistically significant difference was determined between the two cell lines.

### C. Cancer cell adhesion on inflamed endothelial cells under whole blood flow

Leukocyte recruitment at inflamed tissues has a number of similarities with the colonization at distant sites of CTCs. In particular, just like for leukocytes, CTCs tend to transiently interact with the blood vessel walls engaging specific receptor molecules, then adhere and spread over the endothelial cells and, eventually, cross the vascular barrier relocating in the extravascular space. Adhesion molecules are over-expressed in postcapillary venules during an inflammatory process (Granger and Senchenkova, 2010; Strell and Entschladen, 2008; and McEver and Zhu, 2010). Moreover, it is well recognized that leukocyte rolling and adhesion on the inflamed vascular endothelium is modulated by the presence of red blood cells (RBCs). Specifically, experimental observation and simulations have shown that the deformability and shape of RBCs allow them to concentrate within the core of blood vessels leaving a so-called “cell free layer” next to the vessel walls (Goldsmith *et al.*, 1989; Pappu and Bagchi, 2007; Fedosov *et al.*, 2014; and Firrell and Lipowsky, 1989). Leukocytes, which are two-times larger and far less abundant than RBCs, tend to be pushed laterally in the cell free layer by the fast moving RBCs. This process, known as “marginination,” should also affect the vascular behavior of CTCs.

In this section, cancer cell rolling and adhesion over a monolayer of HUVECs is analyzed in the presence of whole blood. The single-channel microfluidic chip was again covered by a confluent monolayer of HUVECs, which were unstimulated or stimulated with TNF- $\alpha$  (12 h only), and cancer cells re-suspended in whole blood were directly injected at two different flow

rates ( $Q = 50$  and  $100$  nl/min). Whole blood, freshly drawn from rats, contained all the cell and molecular components of blood, including red blood cells, platelets, leucocytes and plasma proteins which may all contribute, at different extents, to cancer cell rolling and adhesion (Gay and Felding-Habermann, 2011; Borsig *et al.*, 2002). A fixed hematocrit of 40% was considered. Results for eight different working conditions are provided in Figs. 4(b) and 4(d), which are for  $Q = 50$  and  $100$  nl/min, respectively. As previously, breast cancer cells are identified by blue bars whereas colon cancer cells are associated with red bars. On the left hand side [Figs. 4(a) and 4(c)], representative fluorescence microscopy images are shown for unstimulated HUVECs ( $-TNF-\alpha$ ), and 12 h-stimulated HUVECs ( $+TNF-\alpha$  12 h). The results unequivocally showed that blood cells favor the adhesion of circulating tumor cells to the vascular walls, especially in the

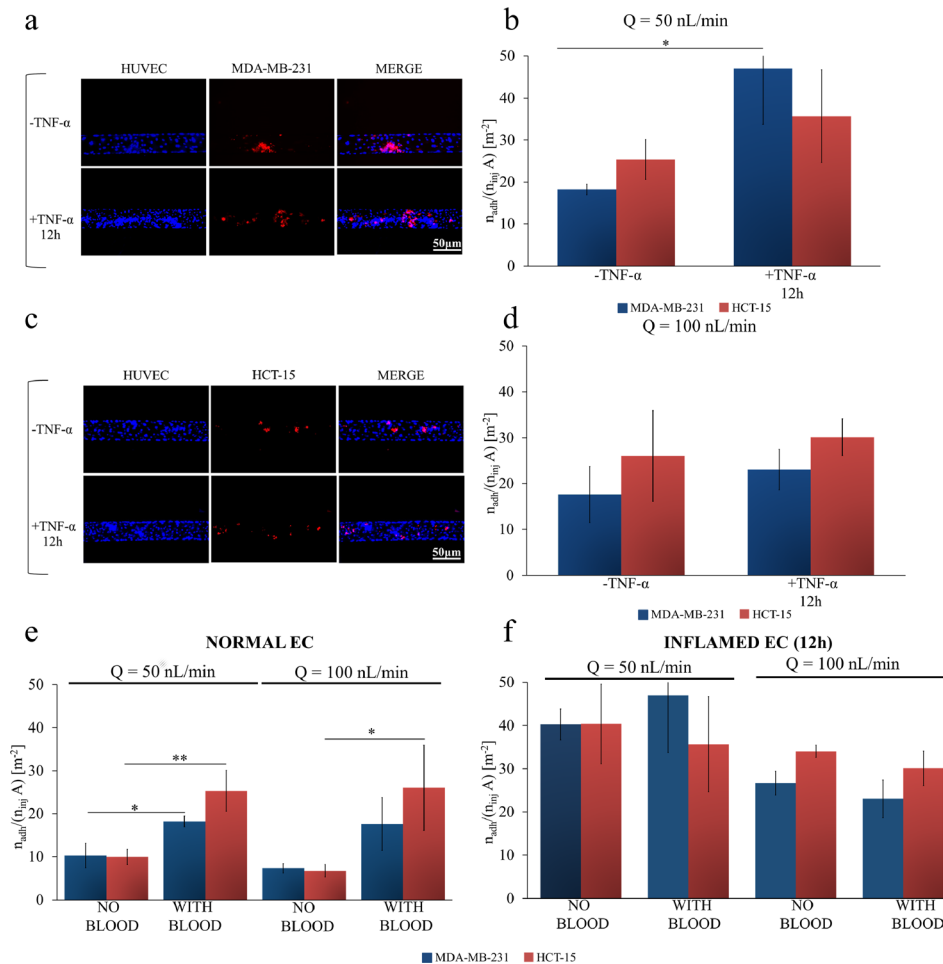


FIG. 4. Cancer cell adhesion on inflamed endothelial cells under whole blood flow. (a) Representative fluorescence microscopy images of breast cancer cells MDA-MB-231 (cell membrane labeled in red with CM-DIL) flowing in whole blood and interacting, in a single-channel microfluidic chip, with a confluent monolayer of HUVECs (cell nuclei stained in blue with DAPI). (b) Normalized number of adhering cancer cells on a HUVEC monolayer of colon cancer HCT-15 (red column) and breast cancer cells MDA-MB-231 (blue column) at a flow rate (50 nl/min), with and without stimulation with  $TNF-\alpha$  (25 ng/ml) in the presence of whole blood (hematocrit: 40%). (c) Representative fluorescence microscopy images of colon cancer cells HCT-15 (cell membrane labeled in red with CM-DIL) flowing in whole blood interacting, in a single-channel microfluidic chip, with a confluent monolayer of HUVECs (cell nuclei stained in blue with DAPI). (d) Normalized number of adhering cancer cells on a HUVEC monolayer of colon cancer cells HCT-15 (red column) and breast cancer cells MDA-MB-231 (blue column) at high flow rate (100 nl/min), with and without stimulation with  $TNF-\alpha$  (25 ng/ml) in the presence of whole blood (hematocrit: 40%). (e) and (f) Normalized number of adhering colon cancer cells HCT-15 (red column) and breast cancer cells MDA-MB-231 (blue column) on a HUVEC monolayer, without (f) and with (e) stimulation of  $TNF-\alpha$  (25 ng/ml) for 12 h at a flow rate of 50 nl/min and 100 nl/min, with and without whole blood (hematocrit: 40%) [Data are plotted as mean  $\pm$  SD.  $n = 3$ . Statistical analysis ANOVA: \* symbol denotes statistically significant difference  $p < 0.05$ ; \*\* symbol denotes statistically significant difference  $p < 0.01$  ( $n_{inj} = 10^6$  cells and  $A = 1.22 \times 10^{-6} m^2$ )].

case of unstimulated endothelium. In Figs. 4(b) and 4(d), the normalized number of adhering cells is reported. At  $Q = 50$  nl/min, the normalized number of adhering HCT-15 and MDA-MB-231 cells was  $25.33 \pm 4.762$  and  $18.19 \pm 1.269$  #/m<sup>2</sup> in control experiments,  $35.68 \pm 10.99$  and  $46.96 \pm 13.18$  #/m<sup>2</sup> after 12 h of TNF- $\alpha$  stimulation, respectively. At  $Q = 100$  nl/min, the normalized number of adhering HCT-15 and MDA-MB-231 cells was  $26.04 \pm 9.90$  and  $17.59 \pm 6.129$  #/m<sup>2</sup> in control experiments,  $30.12 \pm 4.011$  and  $23.04 \pm 4.406$  #/m<sup>2</sup> after 12 h of TNF- $\alpha$  stimulation, respectively. Notably, even under these conditions, no statistically significant difference in cell adhesion was detected between breast and colon cancer cells. Interestingly, a statically significant difference was measured only between untreated and TNF- $\alpha$  treated endothelial cells at the lowest flow rate [ $Q = 50$  nl/min, in Fig. 4(b)]. At highest flow rates, the absolute number of adhering cells reduces and 12 h TNF- $\alpha$  stimulation is insufficient to induce a statistically significant increase in cell deposition.

A direct comparison in terms of CTC vascular adhesion between whole blood flow and physiological solution is now needed. Figures 4(e) and 4(f) collect all the data required for this comparison. Within an unstimulated microvascular network, the presence of blood cells does dramatically increase CTC adhesion [Fig. 4(e)]. For  $Q = 50$  nl/min, the density of firmly adhering CTCs grows from about 10 to 20 #/m<sup>2</sup> moving from physiological solution to whole blood flow. A slightly larger increase is observed for  $Q = 100$  nl/min. Differently, within an inflamed microvascular network, the presence of blood cells does not significantly affect CTC adhesion [Fig. 4(f)]. The density of firmly adhering CTCs is around 40 #/m<sup>2</sup> at 50 nl/min and reduces to about 30 #/m<sup>2</sup> at 100 nl/min, with and without RBCs. This could be interpreted as, under the current conditions, the density of adhering CTCs on the inflamed endothelium has reached saturation and the presence of RBCs cannot further foster cell deposition. Also, RBC-CTC collisions could limit any further increase in cell deposition. Indeed, additional experiments would be needed to support this hypothesis. Interestingly, a direct comparison of the data presented in Figs. 4(e) and 4(f) would lead one to infer that, at higher flow rates (100 nl/min), the density of firmly adhering CTCs on the inflamed and normal vasculature is comparable when a whole blood flow is considered. Again, this could be due to a balance between shear stresses and cell-cell collisions. Indeed, this is not observed at low flow rates (50 nl/min), where adhesion is higher on inflamed endothelium.

These data confirm that blood cells facilitate the vascular adhesion of CTCs, just like for leukocytes, and open up to the following two considerations: CTCs would tend to adhere throughout the microvasculature, on both inflamed and not inflamed endothelial cells, thus increasing the likelihood of finding proper conditions for colonization; in microfluidic experiments, neglecting the role of blood cells could dramatically underestimate the adhesion propensity of CTCs.

#### D. Predicting cancer cell adhesion and rolling on inflamed endothelial cells

In order to predict CTC vascular behavior under different flow and adhesion conditions, a computational model was employed based on previous works by the authors (Decuzzi and Ferrari, 2006; Coclite *et al.*, 2016; and Coclite *et al.*, 2017). In this model, cancer cells were considered as rigid and deformable circular objects exposed to a Poiseuille flow and capable of interacting with vascular walls (endothelial cells) via specific ligand-receptor bonds [Fig. 5(a)]. Simulations were performed in a rectangular computational domain, with height  $H$  ( $= 42 \mu\text{m}$ ) and length  $10H$ , resembling the longitudinal cross section of the single channel in the microfluidic chip. The diameter of cancer cells was fixed to  $d = 15 \mu\text{m}$ , as quantified via bright field microscopy (supplementary Fig. 3). The ratio between the number of ligands decorating the surface of cancer cells and the number of receptors expressed on the endothelium is  $\rho_1$ . Two different ratios  $\rho_1$  were considered, namely, 0.3 and 0.6. These assumed ligand densities return a good agreement between the experimental and numerical predictions for the cell rolling velocity over three different flow rates.

At first, cancer cells were assumed to be rigid, which is indeed the simplest possible hypothesis. Then, simulations were performed for estimating the rolling velocities of cancer



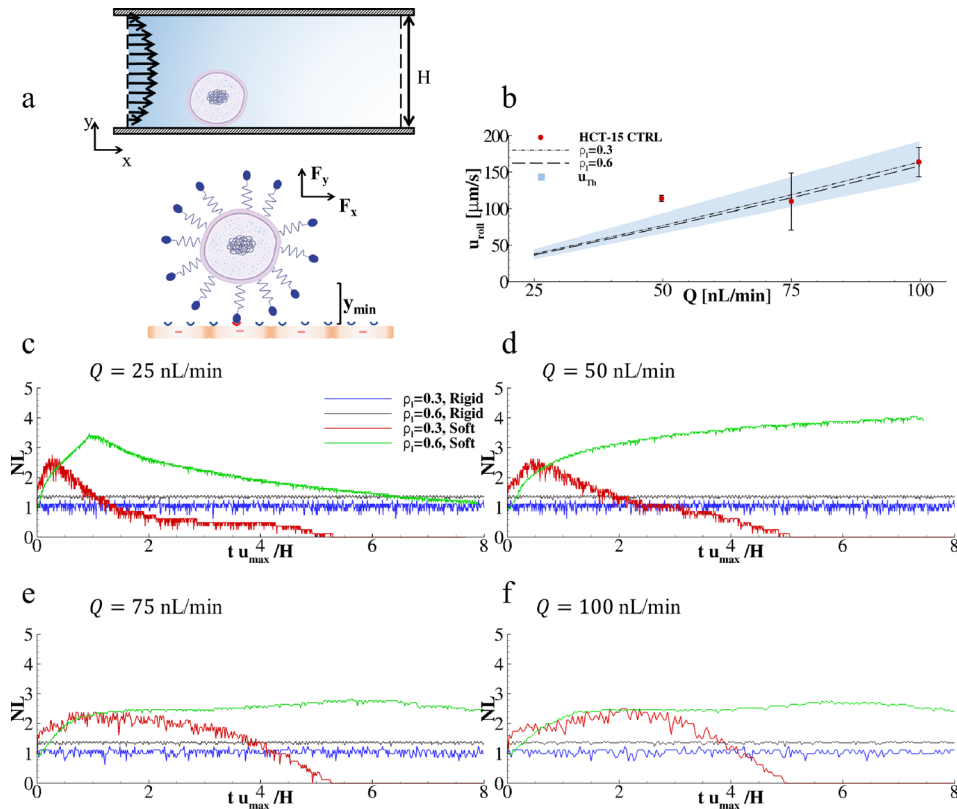


FIG. 5. Predicting cancer cell adhesion and rolling on inflamed endothelial cells. (a) Schematic diagram presenting the computational problem with a close-up depicting ligand-receptor interactions at the interface between cancer (up) and endothelial (lower) cells. (b) Rolling velocities of cancer cells under four different flow rates ( $Q = 25, 50, 75,$  and  $100$  nL/min) and two ligand-receptor bond concentrations ( $\rho_l = 0.3$  and  $0.6$ ) (Solid lines are simulated values, dots are experimental values, and dashed lines are theoretical values). (c)–(f) Variation of the number of active ligand-receptor bonds over time, under four different flow rates ( $Q = 25, 50, 75,$  and  $100$  nL/min), two ligand-receptor bond concentrations ( $\rho_l = 0.3$  and  $0.6$ ), and for soft and rigid cancer cells.  $N_l$  is the number of closed bonds in each time step. This number is computed as the ratio between the current number of closed bonds over the number of closed bonds in the initial configuration.

cells over the vascular wall as a function of four different flow rates, namely,  $Q = 25, 50, 75,$  and  $100$  nL/min; and two  $\rho_l$  ratios, namely,  $0.3$  and  $0.6$ . The resulting data are shown in Fig. 5(b) (lines) where a direct comparison with the corresponding experimental data is also included (blue dots for HCT-15 cells). From the simulations, the cell rolling velocity was predicted to grow quasi-linearly with the flow rate  $Q$  ( $R^2 = 0.998$  and  $0.994$  for  $\rho_l = 0.3$  and  $0.6$ , respectively) and slightly decrease with an increase in  $\rho_l = 0.3$ . Overall, the predicted rolling velocities were found to be in good agreement with the experimental data for  $Q = 100$  nL/min, returning a relative error smaller than  $0.74\%$  and  $3.10\%$  for  $\rho_l = 0.3$  and  $0.6$ , respectively. A larger difference was observed at low flow rates,  $Q = 50$  nL/min, where the relative error increased to about  $43.01\%$  and  $52.07\%$  for  $\rho_l = 0.3$  and  $0.6$ , respectively. This might be due to the fact that this flow rate is very close to the lower limit for the syringe pump used in the experiments. Note that an increase in  $\rho_l$  from  $0.3$  to  $0.6$  was associated with only a  $3.5\%$  decrease in rolling velocity. This is also in agreement with the experimental data of Figs. 3(a) and 3(b) documenting a modest variation in  $u_{roll}$  with vascular inflammation.

Although the “rigid cell” approximation quite accurately modeled the rolling behavior of cancer cells, it could not predict their firm vascular adhesion. Therefore, in a second set of simulations, the cancer cell was considered as a deformable capsule characterized by the dimensionless capillary number  $Ca = 10^{-2}$ . These data are plotted in Figs. 5(c) and 5(f) for four different flow rates ( $Q = 25, 50, 75,$  and  $100$  nL/min) and two ligand-receptor densities ( $\rho_l = 0.3$  and  $0.6$ ). Also, a direct comparison between rigid and soft cells is provided. Soft cells exhibited

more complex vascular adhesion patterns. For  $\rho_l = 0.3$ , soft cells were observed to establish an initial adhesive contact with the endothelial surface resulting in partial cell deformation and increase in the number of ligand-receptor bonds. However, after reaching a maximum, the adhesive interactions were not sufficient to counteract the dislodging hydrodynamic forces and, consequently, the number of close bonds reduced tending eventually to zero. For  $\rho_l = 0.6$ , a larger number of ligand-receptor bonds could be formed leading to stronger adhesive interactions. This is indeed observed in the plots of Figs. 5(c) and 5(f). Also, for sufficiently high flow rates ( $Q \geq 50$  nl/min), partially adhering soft cells were deformed and pushed down to the wall thus maximizing their adhesive surface and interface forces and leading to a 2 to 3-times higher number of ligand-receptor bonds as compared to the corresponding rigid cell cases [Figs. 5(e) and 5(f)]. Notably, simulations predicted that rigid cells would roll over the endothelium with a rolling velocity decreasing with an increasing surface density of ligands [black and blue lines in Figs. 5(c) and 5(f)]. Differently, deformable cells would, for low ligand surface densities, transiently adhere, detach, and move away from the wall pushed by hydrodynamic lift forces [red lines in Figs. 5(c) and 5(f)]; whereas, for high ligand surface densities, deformable cells would firmly adhere, deform under flow, and increase the surface of adhesion as documented by the growth of the number of the engaged ligand-receptor bonds [green lines in Figs. 5(c), 5(f), and supplementary Fig. 4]. Although the present simulations can quite accurately predict the rolling velocities of circulating cancer cells, it should be emphasized that only a fully 3D model, including deformable RBCs and CTCs, could realistically predict the vascular behavior of cancer cells (Fedosov *et al.*, 2011; Muller *et al.*, 2014).

### III. CONCLUSIONS

A microfluidic chip was used to analyze the vascular transport of circulating tumor cells under different biophysical conditions. The surface density of adhering cells and the velocity of rolling cells were quantitatively characterized over a confluent endothelial monolayer as a function of the level of inflammation (no TNF- $\alpha$ ; TNF- $\alpha$  stimulation for 6 h; and TNF- $\alpha$  stimulation for 12 h); flow rate (50 and 100 nl/min); and working fluid (physiological solution and whole blood, at 40% hematocrit). Two different types of cancer cells—colorectal HCT-15 and breast cancer MDA-MB-231 cells—were considered.

It was confirmed that vascular inflammation facilitates cell adhesion in a way proportional to TNF- $\alpha$  stimulation, whereas high flow rates are associated with lower cell deposition. Rolling velocities are only slightly affected by vascular inflammation and grow proportionally with the flow rate. As compared to a physiological solution, flowing cancer cells in whole blood enhances their firm deposition on healthy endothelium rather than on the inflamed vasculature, for all tested conditions. No statistically significant difference is observed for adhesion and rolling between HCT-15 and MDA-MB-231 cells.

These results would imply that neglecting the contribution of whole blood in the analysis of cancer cell dynamics can significantly underestimate their vascular deposition. Furthermore, it can be concluded that whole blood flow supports cancer cell deposition and facilitates metastatization over the entire microvasculature.

### IV. EXPERIMENTAL

#### A. Fabrication of a single channel microfluidic chip

The single channel microfluidic chip was fabricated following protocols previously demonstrated by the authors (Manneschi *et al.*, 2016). Briefly, a SU8-50 master was used as a mold for PDMS replicas of the chip. First, a 40  $\mu\text{m}$  thick layer of SU8-50 photoresist (MicroChem) was spin coated on a silicon wafer (4 in.-P doped-(100)-10–20  $\Omega/\text{cm}^2$ –525  $\mu\text{m}$  thick, from Si-Mat) at 2000 rpm for 30 s. Then, the negative SU8-50 template was pre- and soft baked for solvent evaporation; exposed to UV light and baked again for epoxy crosslinking; and finally developed. This template was replicated using a mixture of PDMS and curing agent Sylgard 182 (Dow Corning Corporation), with a ratio (w:w) 10:1. Specifically, the mixture was poured

on the SU8–50 template, cured in an oven at 60 °C for 15 h, and moved at –20 °C for 1 h. After peeling off from the template, the channel extremities of the PDMS replica were punched via a biopsy puncher (OD = 1 mm, Miltex) to form inlet and outlet ports. Finally, upon oxygen plasma treatment (Pressure = 0.5 mBar, Power = 15 W, Time = 15 s; Plasma System Tucano, Gambetti), PDMS replica was sealed with a glass slide (20 × 60 × 0.17 mm) (No. 1.5H, Deckaläser). The resulting microfluidic chip has a rectangular cross section with a width  $w = 210 \mu\text{m}$ , height  $h = 42 \mu\text{m}$ , and a port-to port length  $l = 2.7 \text{ cm}$ .

### B. Seeding of endothelial cells into the microfluidic chip

Chips were sterilized by autoclave, dried, and covered with 20  $\mu\text{g/ml}$  of fibronectin to allow cell adhesion. HUVECs were introduced in the channel from the inlet port at a density of  $3 \times 10^6$  cells/ml by using a pipette tip. Then, chips were placed in an incubator, to allow cell attachment and growth, and continuously perfused with endothelial cell growth medium supplement-mix (PROMOCELL) until cell confluency was achieved. HUVEC monolayers were inflamed, at the occurrence, with 25 ng/ml of TNF- $\alpha$  for 6 or 12 h. Each experiment was compared to untreated HUVEC monolayer (-TNF- $\alpha$ ).

### C. Cancer cell adhesion and rolling under dynamic conditions

The microfluidic chip was placed on the stage of an epi-fluorescence inverted microscope (Leica 6000). The working fluid was injected into the chip using a syringe pump 33 Dual (Harvard apparatus). After the trypsinization, the cancer cells were incubated for 30 min with CM-DIL, at 37 °C (0.5%, Thermofisher) according to the manufacture's protocol. Then, the cells were washed 3 times with PBS 1× (GIBCO) to remove the excess dye. Finally, the cells were re-suspended in the RPMI medium (HCT-15) or EMEM medium (MDA-MB-231), without FBS, that could interfere with the cell adhesion parameters, at  $1 \times 10^6$  cells/ml. After each rolling experiment, a washing with PBS was performed to remove the non-adherent cancer cells from the endothelium. Tumor cells were introduced via a syringe pump on the HUVEC monolayer inside the single channel chip. The inlet port of the chip was connected to the syringe pump through a polyethylene tube (BTPE-60, Instech Laboratories), while the tube of the outlet port was in PBS, to ensure flow equilibrium. After 1 min of flow, the interaction of tumor cells with HUVECs was recorded for 15 consecutive minutes for each experiment. Two flow rates  $Q$  were imposed via the syringe pump, namely, 50 and 100 nl/min. The resulting rolling velocity of tumor cells was calculated offline by post processing the videos, using the distance traveled by the cell and divided by the time, within a region of interest (ROI) (magnification 10×,  $A = 1.22 \times 10^{-6} \text{ m}^2$ ). At least 15 cancer cells per experiment were monitored. Each experiment was repeated three times for each different conditions and flow rates. For the study of cell adhesion under whole blood flow, the working fluid was obtained by combining a cancer cell suspension (density of  $10^6$  cells/ml) with whole blood from rat, collected in a standard blood test tubing containing 3.2% of buffered citrate to prevent clotting. The working hematocrit was fixed to 40%. Experiments and image acquisition were performed as described above.

### SUPPLEMENTARY MATERIAL

See [supplementary material](#) for the complete description of the materials and methods used in the cell culturing, CTCs adhesion measurement in static and dynamic conditions, and computational modelling. Supplementary material include also supporting figures and movies about CTCs adhesion and rolling on inflamed endothelium, the computed adhesion mechanics of deformable cells, and confocal microscopy images of the adhesion molecules in the microfluidic chip.

### ACKNOWLEDGMENTS

This project was partially supported by the European Research Council, under the European Union's Seventh Framework Programme (FP7/2007-2013)/ERC Grant Agreement No. 616695 and the AIRC (Italian Association for Cancer Research) under the individual investigator Grant No.

17664. The authors acknowledge the precious support provided by the Nikon Center at the Italian Institute of Technology for microscopy acquisitions and analyses. The authors acknowledge the help of Dr. Federica Piccardi with the whole blood experiments. L.P. acknowledges affiliation with A.Li.Sa., Public Health Agency (Liguria Region). A.D.C. acknowledges affiliation with the Wolfson Institute of Preventive Medicine of the Queen Mary University in London (UK) and the Division of Cancer Prevention and Genetics at the European Institute of Oncology in Milan (Italy).

The authors declare that they have no competing interests.

- Barthel, S. R., Gavino, J. D., Descheny, L., and Dimitroff, C. J., "Targeting selectins and selectin ligands in inflammation and cancer," *Expert Opin. Ther. Targets* **11**, 1473–1491 (2007).
- Bersini, S., Jeon, J. S., Dubini, G., Arrigoni, C., Chung, S., Charest, J. L., Moretti, M., and Kamm, R. D., "A microfluidic 3D in vitro model for specificity of breast cancer metastasis to bone," *Biomaterials* **35**, 2454–2461 (2014).
- Borsig, L., Wong, R., Hynes, R. O., Varki, N. M., and Varki, A., "Synergistic effects of L- and P-selectin in facilitating tumor metastasis can involve non-mucin ligands and implicate leukocytes as enhancers of metastasis," *Proc. Natl. Acad. Sci. U. S. A.* **99**, 2193–2198 (2002).
- Burdick, M. M., McCaffery, J. M., Kim, Y. S., Bochner, B. S., and Konstantopoulos, K., "Colon carcinoma cell glycolipids, integrins, and other glycoproteins mediate adhesion to HUVECs under flow," *Am. J. Physiol. Cell Physiol.* **284**, C977–C987 (2003).
- Chaffer, C. L. and Weinberg, R. A., "A perspective on cancer cell metastasis," *Science* **331**, 1559–1564 (2011).
- Coclite, A., de Tullio, M. D., Pascasio, G., and Decuzzi, P., "A combined Lattice Boltzmann and Immersed boundary approach for predicting the vascular transport of differently shaped particles," *Comput. Fluids* **136**, 260–271 (2016).
- Coclite, A., Mollica, H., Rinaldo, S., Pascasio, G., de Tullio, M. D., and Decuzzi, P., "Predicting different adhesive regimens of circulating particles at blood capillary walls," *Microfluid. Nanofluid.* **21**, 168 (2017).
- Decuzzi, P. and Ferrari, M., "The adhesive strength of non-spherical particles mediated by specific interactions," *Biomaterials* **27**, 5307–5314 (2006).
- Fedosov, D. A., Noguchi, H., and Gompper, G., "Multiscale modeling of blood flow: From single cells to blood rheology," *Biomech. Model. Mechanobiol.* **13**, 239–258 (2014).
- Fedosov, D. A., Caswell, B., and Karniadakis, G. E., "Wall shear stress-based model for adhesive dynamics of red blood cells in malaria," *Biophys. J.* **100**, 2084–2093 (2011).
- Fidler, I. J., "Metastasis: Quantitative analysis of distribution and fate of tumor emboli labeled with <sup>125</sup>I-5-iodo-2'-deoxyuridine," *J. Natl. Cancer Inst.* **45**, 773–782 (1970).
- Firrell, J. C. and Lipowsky, H. H., "Leukocyte margination and deformation in mesenteric venules of rat," *Am. J. Physiol.-Heart Circulatory Phys.* **256**, H1667–H1674 (1989).
- Flatmark, K., Maelsandsmo, G. M., Martinsen, M., Rasmussen, H., and Fodstad, O., "Twelve colorectal cancer cell lines exhibit highly variable growth and metastatic capacities in an orthotopic model in nude mice," *Eur. J. Cancer* **40**, 1593–1598 (2004).
- Gay, L. J. and Felding-Habermann, B., "Contribution of platelets to tumour metastasis," *Nat. Rev. Cancer* **11**, 123–134 (2011).
- Goldsmith, H. L., Cokelet, G. R., and Gaehetgens, P., "Robin Fahraeus: Evolution of his concepts in cardiovascular physiology," *Am. J. Physiol.-Heart Circulatory Phys.* **257**, H1005–H1015 (1989).
- Granger, D. N. and Senchenkova, E., "Inflammation and the microcirculation," in *Colloquium Series on Integrated Systems Physiology: From Molecule to Function* (Morgan & Claypool Life Sciences, 2010), pp. 1–87.
- Holliday, D. L. and Speirs, V., "Choosing the right cell line for breast cancer research," *Breast Cancer Res.* **13**, 215 (2011).
- Hood, J. L., San, R. S., and Wickline, S. A., "Exosomes released by melanoma cells prepare sentinel lymph nodes for tumor metastasis," *Cancer Res.* **71**, 3792–3801 (2011).
- Hoshino, A., Costa-Silva, B., Shen, T. L., Rodrigues, G., Hashimoto, A., Tesic Mark, M., Molina, H., Kohsaka, S., Di Giannatale, A., Ceder, S., Singh, S., Williams, C., Sopolop, N., Uryu, K., Pharmed, L., King, T., Bojmar, L., Davies, A. E., Ararso, Y., Zhang, T., Zhang, H., Hernandez, J., Weiss, J. M., Dumont-Cole, V. D., Kramer, K., Wexler, L. H., Narendran, A., Schwartz, G. K., Healey, J. H., Sandstrom, P., Labori, K. J., Kure, E. H., Grandgenett, P. M., Hollingsworth, M. A., de Sousa, M., Kaur, S., Jain, M., Mallya, K., Batra, S. K., Jarnagin, W. R., Brady, M. S., Fodstad, O., Muller, V., Pantel, K., Minn, A. J., Bissell, M. J., Garcia, B. A., Kang, Y., Rajasekhar, V. K., Ghajar, C. M., Matei, I., Peinado, H., Bromberg, J., and Lyden, D., "Tumour exosome integrins determine organotropic metastasis," *Nature* **527**, 329–335 (2015).
- Huang, R., Zheng, W., Liu, W., Zhang, W., Long, Y., and Jiang, X., "Investigation of tumor cell behaviors on a vascular microenvironment-mimicking microfluidic chip," *Sci. Rep.* **5**, 17768 (2015).
- Jeon, J. S., Bersini, S., Gilardi, M., Dubini, G., Charest, J. L., Moretti, M., and Kamm, R. D., "Human 3D vascularized organotypic microfluidic assays to study breast cancer cell extravasation," *Proc. Natl. Acad. Sci. U. S. A.* **112**, 214–219 (2015).
- Joyce, J. A. and Pollard, J. W., "Microenvironmental regulation of metastasis," *Nat. Rev. Cancer* **9**, 239–252 (2009).
- Kaplan, R. N., Riba, R. D., Zacharoulis, S., Bramley, A. H., Vincent, L., Costa, C., MacDonald, D. D., Jin, D. K., Shido, K., Kerns, S. A., Zhu, Z., Hicklin, D., Wu, Y., Port, J. L., Altorki, N., Port, E. R., Ruggiero, D., Shmelkov, S. V., Jensen, K. K., Rafii, S., and Lyden, D., "VEGFR1-positive haematopoietic bone marrow progenitors initiate the pre-metastatic niche," *Nature* **438**, 820–827 (2005).
- Kienast, Y., von Baumgarten, L., Fuhrmann, M., Klinkert, W. E., Goldbrunner, R., Herms, J., and Winkler, F., "Real-time imaging reveals the single steps of brain metastasis formation," *Nat. Med.* **16**, 116–122 (2010).
- Kim, S., Takahashi, H., Lin, W. W., Descargues, P., Grivennikov, S., Kim, Y., Luo, J. L., and Karin, M., "Carcinoma-produced factors activate myeloid cells through TLR2 to stimulate metastasis," *Nature* **457**, 102–106 (2009).
- Manneschi, C., Pereira, R. C., Marinaro, G., Bosca, A., Francardi, M., and Decuzzi, P., "A microfluidic platform with permeable walls for the analysis of vascular and extravascular mass transport," *Microfluid. Nanofluid.* **20**, 113 (2016).

- McEver, R. P. and Zhu, C., "Rolling cell adhesion," *Annu. Rev. Cell Dev. Biol.* **26**, 363–396 (2010).
- Muller, K., Fedosov, D. A., and Gompper, G., "Margination of micro- and nano-particles in blood flow and its effect on drug delivery," *Sci. Rep.* **4**, 4871 (2014).
- Myung, J. H., Gajjar, K. A., Pearson, R. M., Launier, C. A., Eddington, D. T., and Hong, S., "Direct measurements on CD24-mediated rolling of human breast cancer MCF-7 cells on E-selectin," *Anal. Chem.* **83**, 1078–1083 (2011).
- Nguyen, D. X., Bos, P. D., and Massague, J., "Metastasis: From dissemination to organ-specific colonization," *Nat. Rev. Cancer* **9**, 274–284 (2009).
- Niu, Y., Bai, J., Kamm, R. D., Wang, Y., and Wang, C., "Validating antimetastatic effects of natural products in an engineered microfluidic platform mimicking tumor microenvironment," *Mol. Pharm.* **11**, 2022–2029 (2014).
- Pappu, V. and Bagchi, P., "Hydrodynamic interaction between erythrocytes and leukocytes affects rheology of blood in microvessels," *Biorheology* **44**, 191–215 (2007).
- Pisano, M., Triacca, V., Barbee, K. A., and Swartz, M. A., "An in vitro model of the tumor-lymphatic microenvironment with simultaneous transendothelial and luminal flows reveals mechanisms of flow enhanced invasion," *Integr. Biol. (Camb)* **7**, 525–533 (2015).
- Popel, A. S. and Johnson, P. C., "Microcirculation and hemorheology," *Annu. Rev. Fluid Mech.* **37**, 43–69 (2005).
- Provenzano, P. P., Eliceiri, K. W., and Keely, P. J., "Multiphoton microscopy and fluorescence lifetime imaging microscopy (FLIM) to monitor metastasis and the tumor microenvironment," *Clin. Exp. Metastasis* **26**, 357–370 (2009).
- Ríos-Navarro, C., de Pablo, C., Collado-Díaz, V., Orden, S., Blas-García, A., Martínez-Cuesta, M. Á., Esplugues, J. V., and Alvarez, A., "Differential effects of anti-TNF- $\alpha$  and anti-IL-12/23 agents on human leukocyte-endothelial cell interactions," *Eur. J. Pharmacol.* **765**, 355–365 (2015).
- Roberts, S. A., Waziri, A. E., and Agrawal, N., "Development of a single-cell migration and extravasation platform through selective surface modification," *Anal. Chem.* **88**, 2770–2776 (2016).
- Schluter, K., Gassmann, P., Enns, A., Korb, T., Hemping-Bovenkerk, A., Holzen, J., and Haier, J., "Organ-specific metastatic tumor cell adhesion and extravasation of colon carcinoma cells with different metastatic potential," *Am. J. Pathol.* **169**, 1064–1073 (2006).
- Shiozawa, Y., Pedersen, E. A., Havens, A. M., Jung, Y., Mishra, A., Joseph, J., Kim, J. K., Patel, L. R., Ying, C., Ziegler, A. M., Pienta, M. J., Song, J., Wang, J., Loberg, R. D., Krebsbach, P. H., Pienta, K. J., and Taichman, R. S., "Human prostate cancer metastases target the hematopoietic stem cell niche to establish footholds in mouse bone marrow," *J. Clin. Invest.* **121**, 1298–1312 (2011).
- Solinas, G., Marchesi, F., Garlanda, C., Mantovani, A., and Allavena, P., "Inflammation-mediated promotion of invasion and metastasis," *Cancer Metastasis Rev.* **29**, 243–248 (2010).
- Song, J. W., Cavnar, S. P., Walker, A. C., Luker, K. E., Gupta, M., Tung, Y. C., Luker, G. D., and Takayama, S., "Microfluidic endothelium for studying the intravascular adhesion of metastatic breast cancer cells," *PLoS One* **4**, e5756 (2009).
- Strell, C. and Entschladen, F., "Extravasation of leukocytes in comparison to tumor cells," *Cell Commun. Signaling* **6**, 10 (2008).
- Talmadge, J. E. and Fidler, I. J., "AACR centennial series: The biology of cancer metastasis: Historical perspective," *Cancer Res.* **70**, 5649–5669 (2010).
- Wang, X. Y., Pei, Y., Xie, M., Jin, Z. H., Xiao, Y. S., Wang, Y., Zhang, L. N., Li, Y., and Huang, W. H., "An artificial blood vessel implanted three-dimensional microsystem for modeling transvascular migration of tumor cells," *Lab Chip* **15**, 1178–1187 (2015).
- Wirtz, D., Konstantopoulos, K., and Searson, P. C., "The physics of cancer: The role of physical interactions and mechanical forces in metastasis," *Nat. Rev. Cancer* **11**, 512–522 (2011).
- Witz, I. P., "The selectin-selectin ligand axis in tumor progression," *Cancer Metastasis Rev.* **27**, 19–30 (2008).
- Zervantonakis, I. K., Hughes-Alford, S. K., Charest, J. L., Condeelis, J. S., Gertler, F. B., and Kamm, R. D., "Three-dimensional microfluidic model for tumor cell intravasation and endothelial barrier function," *Proc. Natl. Acad. Sci. U. S. A.* **109**, 13515–13520 (2012).
- Zhang, Q., Liu, T., and Qin, J., "A microfluidic-based device for study of transendothelial invasion of tumor aggregates in realtime," *Lab Chip* **12**, 2837–2842 (2012).